Toward a 1.54 μm Electrically Driven Erbium-Doped Silicon Slot Waveguide and Optical Amplifier

A. Tengattini, D. Gandolfi, N. Prtljaga, A. Anopchenko, J. M. Ramírez, F. Ferrarese Lupi, Y. Berencén, D. Navarro-Urrios, P. Rivallin, K. Surana, B. Garrido, J.-M. Fedeli, and L. Pavesi

***Abstract*—In this paper, we report on the first attempt to design, fabricate, and test an on-chip optical amplifier which works at 1540 nm and can be electrically driven. It is based on an asymmetric silicon slot waveguide which embeds the active material. This is based on erbium-doped silicon rich silicon oxide. We describe the horizontal asymmetric slot waveguide design which allows us to get a high field confinement in a nanometer thick active layer. In addition, we detail the complex process needed to fabricate the structure. The waveguides have been characterized both electrically as well as optically. Electroluminescence can be excited by hot carrier injection, due to impact excitation of the Er ions. Propagation losses have been measured and high values have been found due to processing defects. Pump and probe measurements show a voltage dependent strong attenuation of the probe signal due to free carrier accumulation and absorption in the slot waveguide region. At the maximum electrical pumping level, electroluminescence signal is in the range of tens of μW/cm^2 and the overall loss of the device is only -6 dB. Despite not demonstrating optical amplification, this study shines some light on the path to achieve an all-silicon electrically driven optical amplifier.**

***Index Terms*—Electroluminescence (EL), erbium, horizontal slot waveguide, silicon photonics.**

I. Introduction

ERBIUM (Er^{3+})-doped silicon-rich-oxide (SRO) films offer a promising material platform for the development of compact waveguide amplifiers and lasers [1], [2]. A particular advantage of this approach with respect to Er^{3+} in glass is given by the possibility of electrical excitation of Er^{3+} [3]. In order to have an efficient electrical injection, very thin films are required [4], [5]. In addition, multilayered SRO structures allow for bipolar direct tunneling [6]. Slot waveguides, where light confinement happens in a thin low refractive index layer sandwiched by two thick high refractive index material, emerge as a natural choice [7]–[9]. The slot geometry allows also for a straightforward electrical contact definition [4], [5], [10].

In this paper, we will present the design, the modeling, the fabrication, and the characterization of slot waveguides for electrically pumped waveguide amplifiers based on erbium-doped material. These have been fabricated in a standard complementary metal–oxide semiconductor (CMOS) fab line.

Manuscript received August 22, 2012; revised November 26, 2012; accepted November 26, 2012. Date of publication November 30, 2012; date of current version December 31, 2012. This work was supported by the European Commission, through the Project ICTFP7-224312 HELIOS and by Italy–Spain integrated actions.

A. Tengattini, D. Gandolfi, N. Prtljaga, A. Anopchenko, and L. Pavesi are with the Nanoscience Laboratory, Department of Physics, University of Trento, 38123 Povo, Italy (e-mail: tengattini@science.unitn.it; d.gandolfi@science.unitn.it; nikolap@science.unitn.it; anopchenko@science.unitn.it; pavesi@science.unitn.it).

J. M. Ramírez, F. Ferrarese Lupi, Y. Berencén, and B. Garrido are with the Departament d'Electronica, Universitat de Barcelona, 08028 Barcelona, Spain (e-mail: jmramirez@el.ub.es; fferrarese@el.ub.es; yberencen@el.ub.es; bgarrido@el.ub.edu).

D. Navarro-Urrios was with the Departament d'Electronica, Universitat de Barcelona, 08028 Barcelona, Spain. He is now with the Catalan Institute of Nanotechnology, 08193 Bellaterra, Spain (e-mail: danielnavarrourrios@gmail.com).

P. Rivallin, K. Surana, and J.-M. Fedeli are with the CEA Grenoble, 38054 Grenoble Cedex, France (e-mail: pierre.mur@cea.fr; kavita.surana@cea.fr; jean-marc.fedeli@cea.fr).

Color versions of one or more of the figures in this paper are available online at http://ieeexplore.ieee.org.

Digital Object Identifier 10.1109/JLT.2012.2231050

II. Design and Simulation

There are two possible slot orientations that could be considered for the realization of a slot waveguide-based amplifier: vertical and horizontal [4], [11]. In the vertical configuration, significant optical losses may be induced by slot wall roughness [4], [12]. Although significant progresses have been made recently [13], [14], multilayered material deposition on side walls remains a rather challenging task even by the conformal growth [12]. On the contrary, horizontal slot Er^{3+}-doped SRO structures, which might also consist of alternating layers of SRO and SiO_2 [15], are easier to deposit and process [17]. Therefore, in this study, we opt for a horizontal slot configuration. Clearly, field enhancement effects due to the slot waveguide geometry are observed for transverse magnetic TM polarization only.

While very precise control of device dimensions can be achieved by using electron beam lithography [12], optical lithography is preferred for industrial applications and mass production. Unfortunately, electrically driven devices have a very complex design, involving multiple lithographic patterning steps [16]. Thus, special attention has to be paid in order to relax optical alignment constrains between different mask levels.

Another relevant issue is the choice of the slot wall material. Monocrystalline silicon has superior electrical and optical properties but it cannot be grown in a CMOS process. It is only available as a substrate or device layer in silicon-on-insulator (SOI) wafers. Consequently, the top slot cladding or even the whole slot waveguide has to be deposited. Polycrystalline silicon (polysilicon) or amorphous silicon can be used [5], [17], polysilicon being better suited for electrically injection devices due to a better electrical mobility [5]. This motivates our choice of a polycrystalline silicon top cladding.

Low optical losses in polysilicon can be achieved by long high temperature annealing in the presence of hydrogen [5]. However, this may be impractical as it may interfere with optimum thermal budget for Er^{3+}-doped SRO films and causes

0733-8724/$31.00 © 2012 IEEE

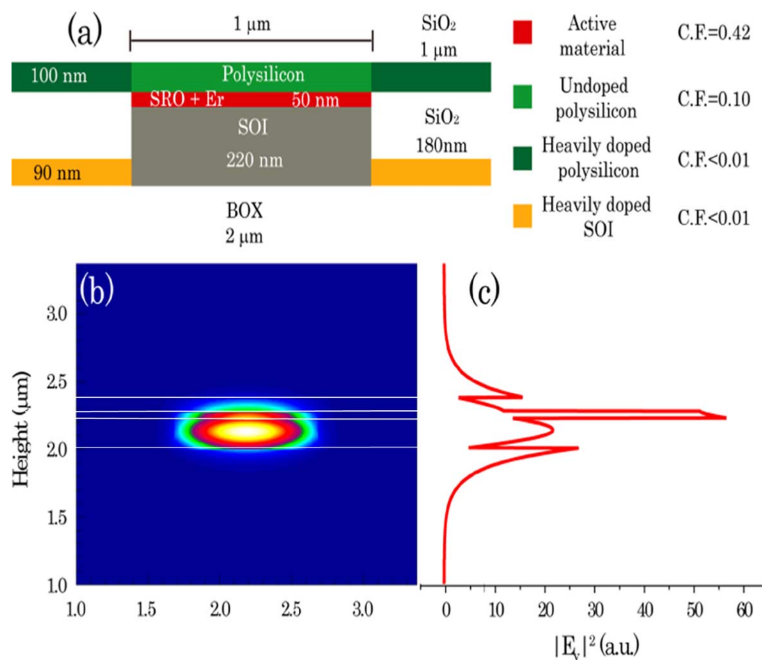

Fig. 1. (a) Schematic of the asymmetric slot waveguide for electrical injection. C.F. stands for confinement factor which gives the fraction of the optical electric field in the indicated area. (b) Intensity profile of the fundamental TM mode. (c) Vertical electric field profile of the fundamental optical TM mode.

dopant out-diffusion. Therefore, to reduce the optical losses, it is more convenient to minimize the fraction of the light guided in the polycrystalline part, while still maintaining a high fraction of field in the slot region. This can be achieved by an asymmetric geometry of the slot waveguide [see Fig. 1(a)]. The asymmetric geometry still allows for a large field fraction in the slot region while minimizing the field in the polysilicon top cladding layer [see Fig. 1(b) and (c)].

The slab character of the polycrystalline silicon top cladding allows for extremely easy lithographic patterning of electrodes since the top polysilicon width does not influence critically the optical waveguiding in the TM polarization.

The structure optimization (layer thicknesses) has been performed with a commercially available fully vectorial mode solver based on the film mode matching method (FIMWAVE, Photon Design). The whole structure is defined on commercially available SOI wafer with a 220 nm thick silicon layer on the top of a buried oxide (BOX) (2 μm thick). The active material thickness in the slot was fixed to 50 nm, an optimum value for a slot waveguide amplifier [18], [20] and a maximum value for which efficient electrical injection in multilayer samples has been demonstrated [3], [19]. Previous reports indicate a maximum Er modal gain of 2 dB/cm in a slot waveguide with 50 nm thick active material [20].

The waveguide width of 1 μm has been chosen in order to increase the active material volume. For this width, the fundamental TM mode displays high confinement in the slot region [see Fig. 1(a)], while the higher order modes exhibits high radiative losses and, practically, do not contribute to light propagation.

The thicknesses of the top cladding and bottom electrodes, which form side slabs named wings in the following, have been chosen in order to maintain good electrical conductivity while still inhibiting the mode leaking towards the wings [see Fig. 1(a) and (b)]. Moreover, as the optical field does not penetrate in wings, doping can be increased providing with good electrical contacts. Additionally, the slot parameters chosen for the fabrication are quite robust with respect to fabrication-induced variations, including the changes of active material thickness or refractive index (different silicon excess, thermal treatments; see Fig. 2).

III. Experimental Details

A. Waveguides Processing

The waveguides have been fabricated on SOI wafers in a 200 mm CMOS pilot line of the CEA, Lèti. The schematics of the typical process flow are reported in Fig. 3. Commercially available SOI wafers with 220 nm of lightly doped p-type Silicon (Si) layer on a 2 μm thick BOX were used for device manufacturing. The device layer was implanted with boron to form a concentration gradient, with high concentration near the BOX and light doping in the proximity of the surface ($10^{17}/cm^3$).

The active layer with a thickness of 50 nm was grown on Si [see Fig. 3(a)]. It consists either of stoichiometric or non-stoichiometric (silicon rich) oxide. Stoichiometric silicon oxide was an high temperature oxide and was used as a reference sample. SRO was deposited by low-pressure chemical vapor deposition (LPCVD) in a multilayer sequence. A layer of 2 nm of silicon dioxide and a layer of 3 nm of SRO, with a nominal silicon content excess of 20%, were repeated ten times. The gases used are N_2O and silane, only the ratio changes for the SiO_2 and the SRO layers. For the SRO step, the time is 16 min and 30 s, with a ratio between the N_2O and the SiH_4 equal to 200/40 sccm, while for the oxide step, the time is 26 min and the ratio between the gases 960/40 sccm.

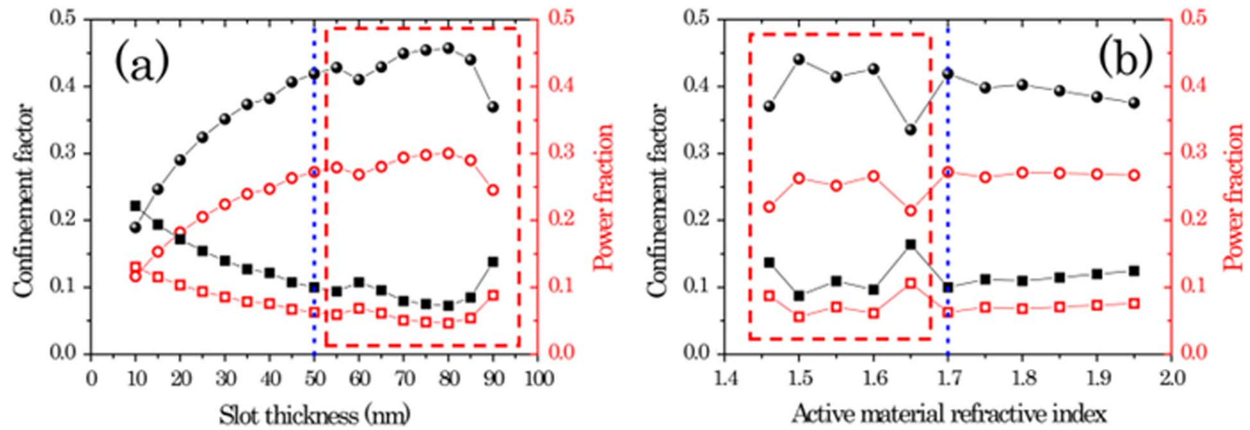

Fig. 2. Confinement factor (black full symbols) and power fraction (red empty symbols) of the fundamental TM mode in the slot region (circles) and polysilicon top cladding (squares) as a function of (a) active material thickness and (b) active material refractive index. Vertical blue-dotted line indicates nominal parameters. Red-dashed square indicates the range of parameters for which fundamental TM mode experiences additional radiative losses due to "leaking" toward the waveguides "wings."

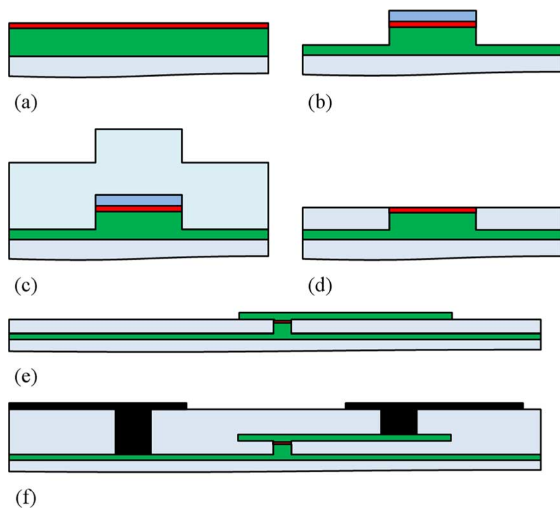

Fig. 3. Schematic overview of the processing steps for the realization of the Er^{3+}-doped electrically driven asymmetric horizontal slot waveguide. (a) Deposition on the lightly boron-doped SOI wafer (light blue—BOX, green—silicon layer) of the active layer (red—Er^{3+}-doped SRO or silica). (b) Waveguide definition by a partial 90 nm etch of the silicon layer on the BOX (the blue layer is a mask layer); (c) Bottom electrode in the wings are implanted with boron, while the mask layer protects the waveguide core; the whole structure is then covered with an oxide. (d) Excess silica and hard mask (blue) are removed in a CMP step. (e) Top polycrystalline silicon cladding is deposited and defined yielding the slot waveguide; (f) Vias openings and metal deposition define the metal contacts (black), for electrical injection in the slot waveguide.

A measured overall silicon content excess in the stack of 8.7% was determined *ex situ* by the X-ray photoelectron spectroscopy. The active layers were then annealed at 900 °C for 1 h. This thermal treatment promotes the phase separation and the silicon nanocluster formation in SRO active layer. TEM analysis shows a loss of layering in the annealed film. Erbium was finally introduced by ion implantation with a dose of $10^{15}/cm^2$ and energy of 20 keV. A peak Er^{3+} concentration of $\approx 3.5 \times 10^{20}/cm^3$ in the center of the active layer was determined by the secondary ion mass spectrometry. Erbium clustering was also observed. Additional details on the active layer morphology are reported in [21].

The waveguide has been defined by etching 90 nm of the silicon layer on the BOX [see Fig. 3(b)]. The waveguide formation is followed by boron implantation into the areas outside the slot region ("wings") and silicon dioxide deposition [see Fig. 3(c)]. The postimplantation annealing is performed at 800 °C for 6 h in order to activate both the Er^{3+} ions and the boron implant. Afterward, the hard mask on the top of the waveguide surface is removed in a chemical–mechanical polishing/planarization (CMP) steps [see Fig. 3(d)]. An undoped top polycrystalline silicon layer 116 nm thick is deposited by LPCVD at 620 °C [see Fig. 3(e)]. The top polysilicon layer is doped outside the slot area (wings) with phosphorus to an electron concentration of $10^{19}/cm^3$. A CMOS compatible Ti/TiN/AlCu metal stack is used for contacts [see Fig. 3(f)].

Fig. 4(a) shows the layout of the fabricated waveguides. The real thickness of the active layer is $\approx$40 nm. To couple the light in and out, the waveguides are ended with an adiabatic taper and a grating coupler. SEM images of cross section of the fabricated waveguide show that the initial design is reproduced in the fabrication [cf., Figs. 4(b) and 1(a)].

In the following, the waveguides containing the layer with the Er^{3+} ions in silica will be labeled as Er:SiO_2, while the ones with the silicon nanocrystals will be labeled as Er:Si-NCs.

B. Measurement Setup

The realized structures have been experimentally characterized, both electrically and optically. The whole setup has been built on a commercial probe station (Suss MicroTec PM8), where both optical and electrical probes have been used. The optical probes have been realized by using single-mode tapered fibers facing the gratings with the optimized input angle (spot diameter of 2.5 ± 0.3 μm at a working distance of 14 ± 2 μm). A photograph of the probes during a measurement is shown in Fig. 5.

The electrical analysis has been performed using a semiconductor device analyzer (Agilent B1500A). The connections to the device are achieved via triaxial cables, terminated with a sharp probe tip contacts. Optical characterization has been done using two different infrared tunable lasers (NetTest Tunics BT

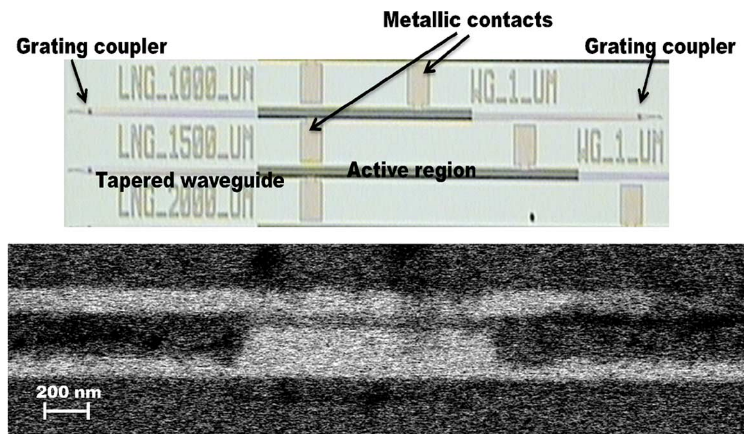

Fig. 4. (a) Top view optical image of the waveguides. Note that Er was implanted only in the region covered by the metal line (label active region). (b) SEM image of the fabricated waveguide cross-section. Dark and light regions correspond to silicon oxide and silicon, respectively.

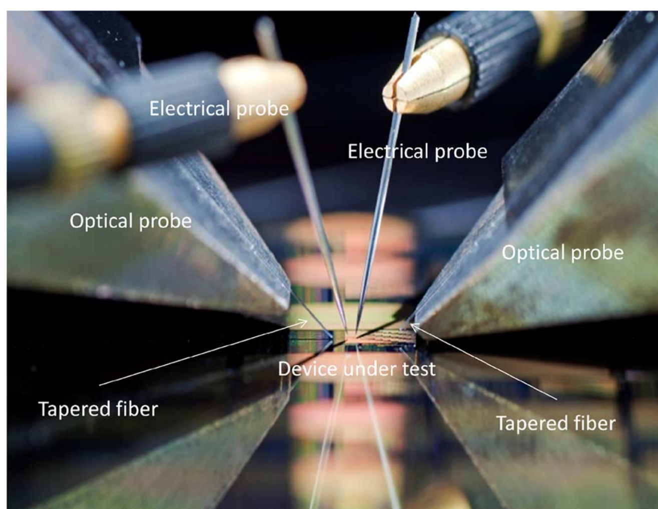

Fig. 5. Details of the experimental setup. The photograph shows a zoom on the measurement region, with the two probes for the electrical contacts and the two infrared tapered fibers for the optical signals.

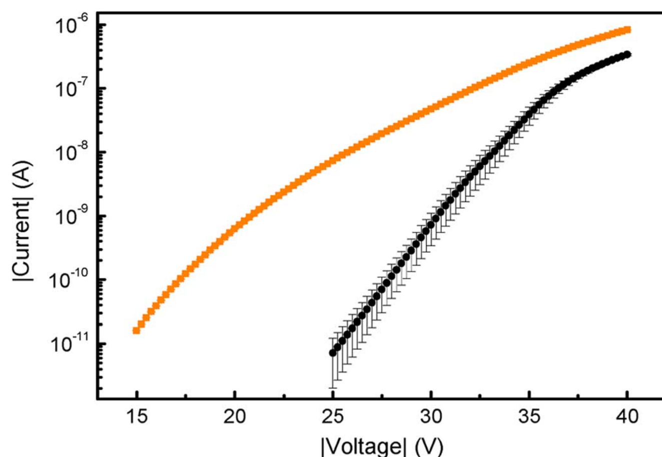

Fig. 6. *I–V* characteristics. The black and the orange lines stand for the Er:SiO_2 and the Er:Si-NCs waveguides, respectively.

or Santec TSL-210F). The transmitted signal is analyzed with an optical spectrum analyzer (OSA Anritsu MS9710B).

To measure electroluminescence (EL), a photon counting module (IdQuantique Id201) is used. As a vision system for alignment purposes, an infrared camera mounted on a microscope has been used.

IV. Experimental Results and Discussion

A. *I–V Characteristics*

Current–voltage (*I–V*) characteristics show a rectifying behavior with a larger conductivity in the Er:Si-NCs waveguides. In forward bias, the silicon nanoclusters enhance the electrical conductivity, leading to higher currents for the same voltage bias (see Fig. 6). On the other hand, these high currents lead to a low breakdown voltage. In fact, while for the Er:Si-NCs waveguides the maximum voltage is around 40 V, for the Er:SiO_2 devices higher voltage (up to 48 V) can be applied without breaking the device. Similar behaviors have been already observed in light-emitting diodes with the same active material [22], [23].

The tunneling current in these waveguides obeys the Fowler–Nordheim law at high injection levels, like the ones shown in Fig. 6 [24]. Therefore, energetic unipolar injection is achieved which eventually yields impact excitation of the Er ions.

B. *Grating Couplers*

First, we characterized the input gratings. This study has been performed by using only one grating and collecting the light directly from the output facet of a cleaved waveguide. The gratings were designed to couple in only TM light which is the one where the field enhancement in the slot region is achieved. The grating coupler pitch and depth are 810 and ≈166 nm, respectively. Indeed only the TM polarized light was transmitted and no light could be detected when the polarization was rotated by 90°. Then, a laser light was scanned in the region between 1500 and 1600 nm and the incident angle is varied to look for optimum coupling efficiency. Fig. 7(a) shows the transmitted intensity at a fixed wavelength of 1540 nm as a function of the incident angle (with respect to the normal). The optimum coupling angle is 25° at which a coupling efficiency of $-(24 \pm 2)$ dB is achieved. Scanning the signal wavelength at this angle the

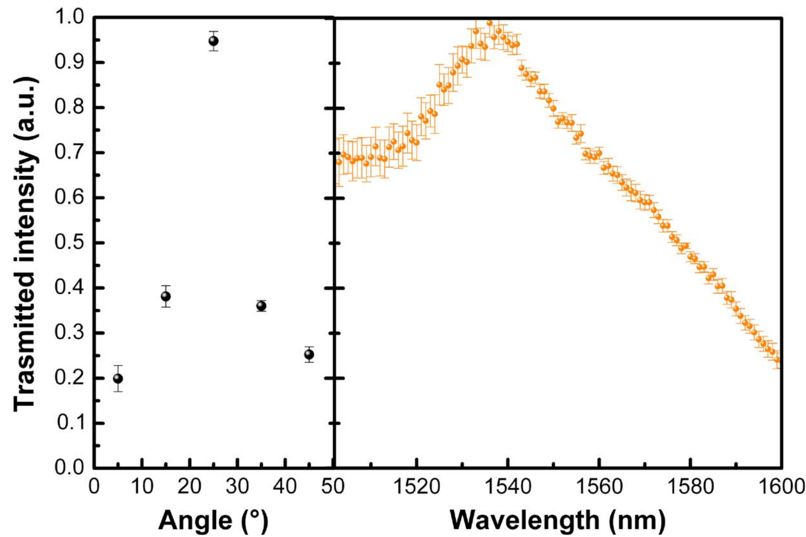

Fig. 7. Transmitted intensity in a 1 mm long waveguide (a) as a function of the incident angle and (b) as a function of the wavelength.

transmission spectrum reported in Fig. 7(b) is obtained. It has to be reported that changing the coupling angle the peak of the transmitted spectrum shifts as expected [25].

C. Propagation Losses

Propagation losses have been evaluated by using waveguides with different lengths (1–3 mm). The propagation losses are (40 ± 5) dB/cm in the region between 1500 and 1600 nm for both waveguide types. No wavelength dependence is observed. Therefore, the Er absorption losses—estimated to 3 dB/cm at 1540 nm [26]—are masked by scattering losses due to processing defects, mainly associated to the CMP process. This is inferred since a significant variation of the propagation losses from die to die on the same wafer has been observed, with fluctuations in excess of ± 20 dB. The random variations in the waveguide thickness due to the imprecise CMP could lead to mode leaking toward the heavily doped wings and, consequently, to combined effect of radiative and free carrier absorption (FCA) losses. This explanation is confirmed by a simple estimation with the values of the FCA in silicon reported in the literature [27]. It is moreover worth mentioning that the scattering/absorption losses in polysilicon top cladding are probably contributing as well, despite the asymmetrical design of the slot waveguides.

D. Electroluminescence

An electro-optical characterization has been performed by monitoring the EL as a function of the applied biasing voltage.

Stronger EL is observed in the devices without the nanoclusters than in the device with the silicon nanoclusters for the same applied voltage. In Fig. 8(a), the EL spectrum when the emission is collected by placing a fiber directly on top of the waveguide is reported. This EL spectrum evidences that we excite the Er ions by impact excitation caused by hot carrier injection. Fig. 8(b) reports the EL collected by a tapered fiber from the output grating as a function of the applied voltage for the Er:SiO_2 waveguides. This shows that light is guided in the active part of the device and emitted from the grating. The voltage range, where the EL signal can be detected, is very small [only 10 V—see Fig. 8(b)]

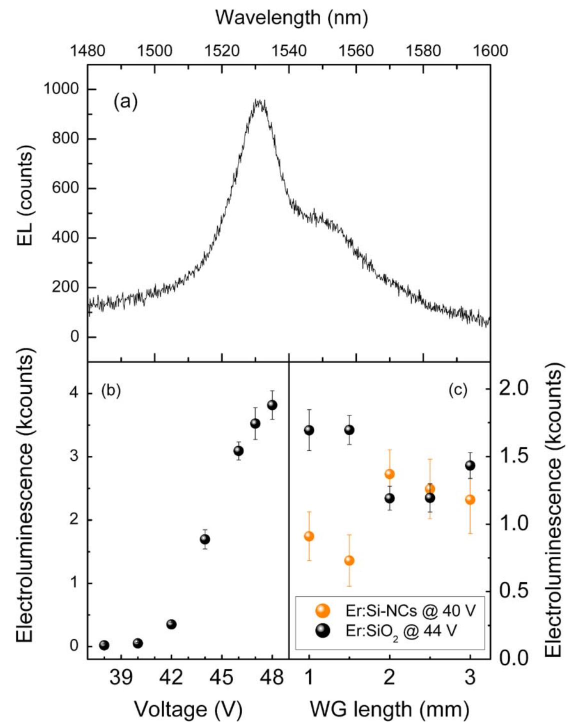

Fig. 8. (a) EL spectra for a voltage of 44 V, collected from the top of the Er:SiO_2 waveguide. (b) EL signal as a function of the applied voltage for the 1 mm long Er:SiO_2 waveguide. Signal is collected at the grating output. (c) EL as a function of the waveguide length for the two different devices at a fixed applied voltage of 40 and 44 V, respectively. Signal is collected at the grating output.

and peaked at high voltages. The optical power density collected is in the range of tens of μW/cm^2, which increases linearly with the electric field applied and superlinearly with the injected current [24]. The optical conversion efficiency, defined as the ratio between the output optical power and the forced electrical power, is equal to 10^{-4}%. Interestingly, the light intensity does not depend appreciably on the waveguide length. Fig. 8(c) shows this dependence for both the Er:SiNCs and the Er:SiO_2 waveguides at a fixed applied voltage, respectively, of 40 and

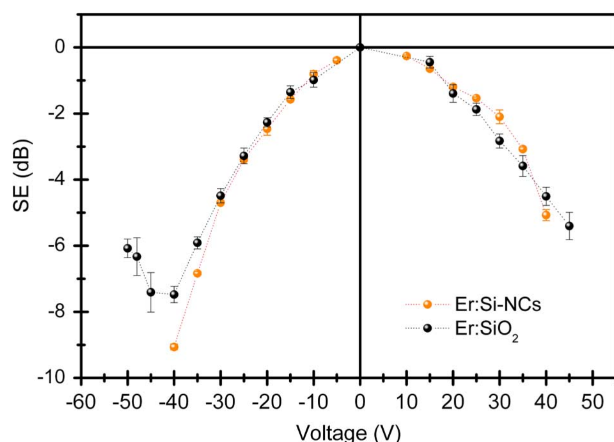

Fig. 9. SE as a function of the applied voltage for the two different waveguides, 1 mm long, at a fixed probing wavelength of 1550 nm.

44 V. These data indicate that the collected emission is coming from a region close to the grating independently on the waveguide length due to the high propagation losses.

E. Pump–Probe Experiment

Finally, we test the transmission of a probe signal as a function of the applied voltage. This experiment could give insights on the suitability of this approach for an on-chip optical amplifier. Fig. 9 shows the ratio between the transmitted signal at an applied bias U versus the transmitted signal for U $= 0$ V—this quantity is usually named signal enhancement (SE). The reported data are for a signal wavelength of 1550 nm and for the Er:Si-NCs waveguides. We observed that the SE decreases for increased bias voltage. No dependence on the signal wavelength is observed too. We attribute this effect to charge accumulation in the Si-NC [28] or defects in the oxide and to the FCA phenomenon, caused by the injected current in the silicon slot waveguide. The losses are higher in forward bias (negative voltage applied to the gate) than in the reverse one, because the injected electron current is higher, too. Very interestingly, in the Er:SiO_2 waveguides, the behavior of the SE is not monotonic, but at higher injection rate, in the forward polarization regime, it starts to increase. This absorption bleaching is observed for voltages lower than -40 V (forward bias), and only for the TM polarization of the input light. The reasons of this interesting behavior are under further investigations. The main point is that the overall loss of the device, at the maximum electrical pumping level, is only -6 dB. We do observe a loss reduction of 2 dB with respect to the optical losses at the lower levels of electrical pumping. However, the magnitude of this enhancement is larger than the maximum estimated enhancement value calculated from the emission cross section of Er^{3+} in this active material and the Er^{3+} concentration. This fact weakens the idea of optical gain and suggests the idea of absorption bleaching, which can be due to various factors (change in electrical transport across device, heating, etc.) influencing the optical losses in the studied devices under high electrical pumping. In fact, the optical losses increase, due to the injected current, because of absorption of the injected charges, accumulation of carriers in the interfaces, and the refractive index change due to the injected carriers. Assuming that the accumulated charges change only the refractive index, for our doping concentration, a change of the refractive index of the order of $\Delta n = 0.01$ is expected [29]. Due to this change, we estimate a maximum increase of the propagation losses of 10 dB/cm, due to the higher overlap of the optical mode with lossy regions of the waveguide. Thus, it can be concluded that the refractive index change is probably of secondary importance with respect to the optical losses induced by FCA and accumulation.

V. Conclusion

Electrically driven erbium-doped slot waveguides, having erbium ions and silicon nanoclusters in the active region, have been designed and fabricated. We do observe guided EL caused by emission from electrically excited erbium ions. Unfortunately, due to the high propagation and FCA losses, no optical amplification has been observed. A necessary condition to develop silicon-based optical amplifiers which exploit Er as active material is to improve significantly the process to reduce the propagation losses. In this paper, we have reported a first attempt in this direction.

Acknowledgment

The authors would like to thank A. Marconi and O. Jambois for the contribution at an early stage of this work and E. Rigo for the photograph of the experimental setup.

References

[1] D. Liang and J. E. Bowers, "Recent progress in lasers on silicon," *Nature Photon.*, vol. 4, no. 8, pp. 511–517, Jul. 2010.
[2] J. D. B. Bradley and M. Pollnau, "Erbium-doped integrated waveguide amplifiers and lasers," *Laser Photon. Rev.*, vol. 5, no. 3, pp. 368–403, May 2011.
[3] O. Jambois, F. Gourbilleau, A. J. Kenyon, J. Montserrat, R. Rizk, and B. Garrido, "Towards population inversion of electrically pumped Er ions sensitized by Si nanoclusters," *Opt. Exp.*, vol. 18, no. 3, pp. 2230–2235, Feb. 2010.
[4] C. A. Barrios and M. Lipson, "Electrically driven silicon resonant light emitting device based on slot-waveguide," *Opt. Exp.*, vol. 13, no. 25, pp. 10092–10101, Dec. 2005.
[5] K. Preston and M. Lipson, "Slot waveguides with polycrystalline silicon for electrical injection," *Opt. Exp.*, vol. 17, no. 3, pp. 1527–1534, Feb. 2009.
[6] A. Marconi, A. Anopchenko, M. Wang, G. Pucker, P. Bellutti, and L. Pavesi, "High power efficiency in Si-nc/SiO_2 multilayer light emitting devices by bipolar direct tunneling," *Appl. Phys. Lett.*, vol. 94, pp. 221110-1–221110-3, 2009.
[7] V. R. Almeida, Q. Xu, C. A. Barrios, and M. Lipson, "Guiding and confining light in void nanostructure," *Opt. Lett.*, vol. 29, no. 11, pp. 1209–1211, Jun. 2004.
[8] Q. Xu, V. R. Almeida, R. R. Panepucci, and M. Lipson, "Experimental demonstration of guiding and confining light in nanometer-size low-refractive-index material," *Opt. Lett.*, vol. 29, no. 14, pp. 1626–1628, Jul. 2004.
[9] Y. C. Jun, R. M. Briggs, H. A. Atwater, and M. L. Brongersma, "Broadband enhancement of light emission in silicon slot waveguides," *Opt. Exp.*, vol. 17, no. 9, pp. 7479–7490, 2009.
[10] P. Muellner, N. Finger, and R. Hainberger, "Lateral leakage in symmetric SOI rib-type slot waveguides," *Opt. Exp.*, vol. 16, no. 1, pp. 287–294, 2008.
[11] P. Sanchis and A. Martinez, "Design of silicon-based slot waveguide configurations for optimum nonlinear performance," *J. Lightw. Technol.*, vol. 25, no. 5, pp. 1298–1305, May 2007.

[12] E. Jordana, J.-M. Fedeli, P. Lyan, J. P. Colonna, P. E. Gautier, N. Daldosso, L. Pavesi, Y. Lebour, P. Pellegrino, B. Garrido, J. Blasco, F. Cuesta-Soto, and P. Sanchis, "Deep-UV lithography fabrication of slot waveguides and sandwiched waveguides for nonlinear applications," in *Proc. 4th IEEE Int. Conf. Group IV Photon.*, 2007, no. 1, pp. 1–3.
[13] R. Ding, T. Baehr-Jones, W.-J. Kim, B. Boyko, R. Bojko, A. Spott, A. Pomerene, C. Hill, W. Reinhardt, and M. Hochberg, "Low-loss asymmetric strip-loaded slot waveguides in silicon-on-insulator," *Appl. Phys. Lett.*, vol. 98, no. 23, pp. 233303-1–233303-3, 2011.
[14] A. Spott, T. Baehr-Jones, R. Ding, Y. Liu, R. Bojko, T. O'Malley, A. Pomerene, C. Hill, W. Reinhardt, and M. Hochberg, "Photolithographically fabricated low-loss asymmetric silicon slot waveguides," *Opt. Exp.*, vol. 19, no. 11, pp. 10950–10958, May 2011.
[15] A. Anopchenko, A. Marconi, E. Moser, S. Prezioso, M. Wang, L. Pavesi, G. Pucker, and P. Bellutti, "Low-voltage onset of electroluminescence in nanocrystalline-Si/SiO_2 multilayers," *J. Appl. Phys.*, vol. 106, no. 3, pp. 033104-1–033104-8, 2009.
[16] T. N. Theis, "The future of interconnection technology," *IBM J. Res. Devel.*, vol. 44, no. 3, pp. 379–390, May 2000.
[17] R. Guider, N. Daldosso, A. Pitanti, E. Jordana, J.-M. Fedeli, and L. Pavesi, "NanoSi low loss horizontal slot waveguides coupled to high Q ring resonators," *Opt. Exp.*, vol. 17, no. 23, pp. 20762–20770, Nov. 2009.
[18] J. T. Robinson, K. Preston, O. Painter, and M. Lipson, "First-principle derivation of gain in high-index-contrast waveguides," *Opt. Exp.*, vol. 16, no. 21, pp. 16659–16669, Oct. 2008.
[19] A. Anopchenko, A. Marconi, M. Wang, G. Pucker, P. Bellutti, and L. Pavesi, "Graded-size Si quantum dot ensembles for efficient light-emitting diodes," *Appl. Phys. Lett.*, vol. 99, no. 18, pp. 181108-1–181108-3, 2011.
[20] G. M. Miller, R. M. Briggs, and H. A. Atwater, "Achieving optical gain in waveguide-confined nanocluster-sensitized erbium by pulsed excitation," *J. Appl. Phys.*, vol. 108, pp. 063109-1–063109-5, 2010.
[21] N. Prtljaga, D. Navarro-Urrios, A. Tengattini, A. Anopchenko, J. M. Ramírez, J. M. Rebled, S. Estradé, J.-P. Colonna, J.-M. Fedeli, B. Garrido, and L. Pavesi, "Limit to the erbium ions emission in silicon rich oxide films by erbium ion clustering," *Opt. Mater. Exp.*, vol. 2, pp. 1278–1285, 2012.
[22] A. Tengattini, A. Marconi, A. Anopchenko, N. Prtljaga, J. M. Ramírez, O. Jambois, Y. Berencén, D. Navarro-Urrios, B. Garrido, F. Milesi, J. Colonna, J.-M. Fedeli, and L. Pavesi, "1.54 μm Er doped light emitting devices: The role of the silicon content," in *Proc. IEEE Int. Conf. Group IV Photon.*, 2011, pp. 77–79.
[23] J. M. Ramírez, F. Ferrarese Lupi, O. Jambois, Y. Berencén, D. Navarro-Urrios, A. Anopchenko, A. Marconi, N. Prtljaga, A. Tengattini, L. Pavesi, J. P. Colonna, J. M. Fedeli, and B. Garrido, "Erbium emission in MOS light emitting devices: From energy transfer to direct impact excitation," *Nanotechnology*, vol. 23, p. 125203, 2012.
[24] J. M. Ramírez, F. F. Lupi, O. Jambois, Y. Berencén, D. Navarro-Urrios, A. Anopchenko, N. Prtljaga, A. Tengattini, L. Pavesi, J. P. Colonna, P. Rivallin, J. M. Fedeli, and B. Garrido, "Er-doped light emitting slot waveguides monolithically integrated in a silicon photonic chip," *Nanotechnology*, 2012, submitted for publication.
[25] D. Taillaert, F. Van Laere, M. Ayre, W. Bogaerts, D. Van Thourhout, P. Bientsman, and R. Baets, "Grating couplers for coupling between optical fibers and nanophotonic waveguides," *Japn. J. Appl. Phys.*, vol. 45, no. 8A, pp. 6071–6077, 2006.
[26] D. Navarro-Urrios, F. Ferrarese Lupi, N. Prtljaga, A. Pitanti, O. Jambois, J. M. Ramírez, Y. Berencén, N. Daldosso, B. Garrido, and L. Pavesi, "Copropagating pump and probe experiments on Si-nc in SiO_2 rib waveguides doped with Er: The optical role of non-emitting ions," *Appl. Phys. Lett.*, vol. 99, pp. 231114-1–231114-3, 2011.
[27] D. K. Schroder, R. N. Thomas, and J. C. Swartz, "Free carrier absorption in silicon," *IEEE Trans. Electron Devices*, vol. ED-25, no. 2, pp. 254–261, Feb. 1978.
[28] D. Navarro-Urrios, A. Pitanti, N. Daldosso, F. Gourbilleau, R. Rizk, G. Pucker, and L. Pavesi, "Quantification of the carrier absorption losses in Si-nanocrystal rich rib waveguides at 1.54 μm," *Appl. Phys. Lett.*, vol. 92, pp. 051101-1–051101-3, 2008.
[29] R. A. Soref and B. R. Bennett, "Electro optical effects in silicon," *IEEE J. Quantum Electron.*, vol. QE-23, no. 1, pp. 123–129, Jan. 1987.

Author biographies not included by author request due to space constraints.